

Contents lists available at ScienceDirect

Journal of Colloid And Interface Science

journal homepage: www.elsevier.com/locate/jcis



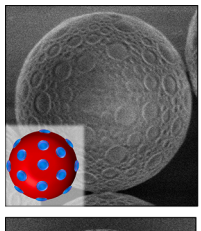


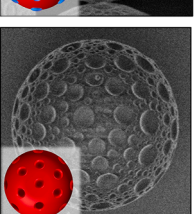
Engineering the surface patchiness and topography of polystyrene colloids: From spheres to ellipsoids

Md Anisur Rahman ^a, Taina Turner ^a, Heather S.C. Hamilton ^b, Laura C. Bradley ^b, Peter J. Beltramo ^{a,*}

- ^a Department of Chemical Engineering, University of Massachusetts Amherst, Amherst, MA 01003, USA
- ^b Department of Polymer Science & Engineering, University of Massachusetts Amherst, Amherst, Massachusetts 01003, USA

G R A P H I C A L A B S T R A C T









ARTICLE INFO

Keywords:
Seeded emulsion polymerization
Polymerization induced phase separation
Colloids
Rough particles
Porous particles
Anisotropic particles
Ellipsoids
Patchy particles

$A\ B\ S\ T\ R\ A\ C\ T$

Hypothesis: Colloidal surface morphology determines suspension properties and applications. While existing methods are effective at generating specific features on spherical particles, an approach extending this to non-spherical particles is currently missing. Synthesizing un-crosslinked polymer microspheres with controlled chemical patchiness would allow subsequent thermomechanical stretching to translate surface topographical features to ellipsoidal particles.

Experiments: A systematic study using seeded emulsion polymerization to create polystyrene (PS) microspheres with controlled surface patches of poly(tert-butyl acrylate) (PtBA) was performed with different polymerization parameters such as concentration of tBA monomer, co-swelling agent, and initiator. Thermomechanical stretching converted seed spheres to microellipsoids. Acid catalyzed hydrolysis (ACH) was performed to remove the patch domains. Roughness was characterized before and after ACH using atomic force microscopy. Findings: PS spheres with controlled chemical patchiness were synthesized. A balance between two factors,

Findings: PS spheres with controlled chemical patchiness were synthesized. A balance between two factors, domain coalescence from reduced viscosity and domain growth via monomer absorption, dictates the final PtBA)

E-mail address: pbeltramo@umass.edu (P.J. Beltramo).

 $^{^{\}ast}$ Corresponding author.

patch features. ACH mediated removal of patch domains produced either golf ball-like porous particles or multicavity particles, depending on the size of the precursor patches. Patchy microspheres were successfully stretched into microellipsoids while retaining their surface characteristics. Particle roughness is governed by the patch geometry and increases after ACH. Overall, this study provides a facile yet controllable platform for creating colloids with highly adjustable surface patterns.

1. Introduction

Colloidal particles with chemical and physical asymmetry have received tremendous attention in recent decades owing to their application in designing materials with improved optical, mechanical, and interfacial properties compared to their isotropic spherical counterparts. The increased interest in synthesizing these symmetry-breaking particles stems from their widespread use as building blocks for the bottomup assembly of materials with advanced functionalities [1–3], including photonic crystals [4–6], and in other applications, such as drug carriers [7], catalyst supports [8,9], compatibilizers [10], coatings [11], superhydrophobic surfaces [12], and Pickering emulsion stabilizers [13]. To that end, numerous efforts have been devoted over the past two decades to fabricate particles with diverse shapes, patterns, surface heterogeneities (chemical or physical), and functionalities. As of now, the achievable anisotropic particles include Janus spheres [14], convexlenses [15], bowls [16], pollen mimics [17], dumbbells [18,19], discs [19,20], patchy [21,22], dimpled [23,24], rough [12,25,26], ellipsoidal [20,27], hemispherical [28], cylindrical particles, [29] and a wide variety of other complex shapes [30,31]. Among them, patchy, dimpled, rough, and ellipsoidal microparticles are particularly promising due to their unique and innovative uses. Glotzer and Solomon [32] characterize these particles with four key anisotropic dimensionality (AD) of patchiness, roughness, faceting, and aspect ratio, and the goal of this work is to combine these different AD into a single synthetic platform where multidimensional anisotropy can be controlled.

Chemical patchiness alone is an intriguing anisotropy dimension due to the potential for bottom-up construction of complex and functional materials [33]. Heterogeneity in surface chemistry due to the patches enable specific interactions at targeted sites on the particle. The final properties of these assemblies are dependent on the size and geometry of the patches [1,34]. They are also promising for drug delivery applications [35] and can be used as model systems to study several liquid state phenomena such as the glass transition, crystallization kinetics, and spinodal decomposition [36-38]. Golf-ball like particles have drawn research interest owing to their distinctive physicochemical and colloidal characteristics, such as elevated surface roughness, increased surface area, special tribological features, enhanced hydrophobicity, and significant light scattering capabilities [23,39]. Creating nonspherical multicavity or polyhedral particles with unique morphologies holds great promise in forming well-defined complex structures, which can potentially be utilized in fabricating photonic crystals [40], special coatings [41], information encryption, as well as enhancing the loading and sustained release of biomolecules [24]. Furthermore, these particles have the ability to undergo assembly with perfectly compatible spherical particles via depletion interactions and centrifugal force to produce molecular mimetic colloidal building blocks that could be used to create metamaterials [24].

Topographical surface heterogeneity, or surface roughness, has been explored as an anisotropy dimension due to the interesting ramifications in the properties of both bulk suspensions and particle laden interfacial systems [42]. Rough colloids can effectively tune the commencement of shear thickening, which is particularly interesting in shock-absorbing materials and slurry processing, by lowering the critical shear rate of thickening in bulk suspensions [43]. Moreover, particle surface roughness also plays an important role in the design and operation of micronanoelectromechanical systems (e.g., nanoswitches, nanoscale tweezers, or actuators) via tailoring the critical Casimir forces that influence

the motion of micro components in such systems [44]. Films created from depositing particles with defined surface roughness exhibit excellent superhydrophobicity [45]. The propulsion speed of rough micromotors experiences a significant increase compared to smooth particles due to the enhanced catalytic loading resulting from the excess surface area caused by surface roughness [46]. Rough particle adsorption to fluid interfaces can lead to controlled capillary interaction [47,48], enhanced interfacial elasticity [49], unexpected particle dynamics [50,51], and assembly structures [47,52,53]. The intriguing behavior shown by particles with defined surface roughness allows the particles not only to improve the stability of Pickering emulsions [54–56] but also to stabilize both oil-in-water and water-in-oil emulsions [57].

On the other hand, shape anisotropy introduces additional advantages that are often complementary to the topographical features described above. Due to shape anisotropy, ellipsoidal particles cause a deformation of the fluid-fluid interface when pinned between two immiscible fluids. This causes long range attractive capillary interactions that can be tuned to assemble particles into defined locally ordered structures having potential application in advanced technologies like displays, sensors, and optoelectronic devices [58]. Shape anisotropy also affords some other features, such as lower percolation threshold, maximum random jammed packing density in 3D environments, and maximum packing fraction in 2D surfaces [59,60], which is beneficial for several applications such as liquid chromatography [61]. While a stable spherical packing only requires six particle—particle interactions, ellipsoids require ten such contacts, making them suitable candidates for building blocks in the development of stronger materials

Several methods have been developed to produce the above mentioned surface anisometric (patchiness, roughness, faceting) polymer particles, including, for example, microfluidic approaches [62–65], template-based fabrication [23,66,67], colloidal assembly [25,68], particle lithography [69], vapor deposition [70,71], in-situ surface reaction [72,73], seeded emulsion polymerization (SEP) [74], and seeded dispersion polymerization [75]. Among these methods, SEP is extremely promising because its high yield in producing scalable and controllable monodisperse particles [76,77] and has the ability to overcome several limitations associated with other methods, such as low yield, inhomogeneous surface heterogeneities, extreme reaction conditions, and lack of reproducibility. Typically, the SEP technique includes the swelling of polymeric seed particles with a second monomer that upon polymerization becomes phase separated in a system known as polymerizationinduced phase separation (PIPS) [77]. However, while successful in producing chemically anisotropic patchy spheres, existing SEP techniques mainly use crosslinked seed particles, [78] which preclude any non-chemical means to introduce shape anisotropy. For example, thermomechanical stretching of crosslinked spheres into ellipsoids fails, restricting the translation of surface patterns onto ellipsoids. Despite the multitude of methods that can produce different types of surface anisotropic particles individually; a remaining challenge exists to synthesizing microparticles with well-controlled chemical and topographical anisotropy in one unified approach.

Colloidal particles that combine multidimensional anisotropy (chemical patchiness, roughness, shape anisotropy) have enormous potential to create highly complex structures. This may be enabled by leveraging properties from each individual anisotropy dimension or emergent properties from combinations of these dimensions [79,80]. Therefore, a detailed understanding of how shape and surface

anisotropies, either combined or individually, contribute to material properties is necessary to exploit anisotropy for advanced materials design and applications, which often face limitations due to the lack of a facile, robust, controllable, and comprehensive synthesis of such particles. Therefore, a method that can produce shape anisotropic particles with surface heterogeneity is highly desired. While manipulating surface patterns on spherical particles is relatively easy, achieving similar functionality on ellipsoidal particles is rather challenging. Only a few examples of patchy ellipsoids exist. Physical vapor deposition has been used to deposit metal patches on ellipsoids, however this approach is poor at controlling the size, number, and distribution of patches [80,81]. Zhang et al [82] synthesized polymeric patchy ellipsoids via wet etching a comb like stabilizer grafted on poly(methyl methacrylate), where the site-directed patchiness and the corresponding properties are highly curvature dependent. Tian et al [83] proposed a strategy for making patchy ellipsoids via double-speed seeded emulsion polymerization technique that involved swelling of poly(glycidyl methacrylate) living seed ellipsoids with styrene; however, the patches were not well controlled. To our knowledge, just one study has been published regarding the synthesis of ellipsoids with rough surfaces [12]. Here, rough ellipsoids were formed by nanoprotrusions stemming from the adsorption of polydopamine nanoparticles that are chemically distinct from the preformed polystyrene (PS) ellipsoids and are not uniformly distributed [12]. Overall, the existing methods of creating surface heterogeneities on ellipsoidal colloids either limited in the achievable surface pattern chemistry, size, and distribution or require complex and multiple steps, and cannot directly be translated from spherical particles.

Herein, we report a comprehensive synthesis technique based on SEP that can produce continuously tunable patchy rough and dimpled spherical particles which can be subsequently stretched into ellipsoids, providing a robust means to transfer chemical and surface topographical features to shape anisotropic ellipsoidal microparticles. To accomplish this, non-crosslinked linear polystyrene seed (LPS) spheres were swelled with a second monomer tert-butyl acrylate (tBA) that upon polymerization gets phase separated from the continuous PS domain yielding patches of poly(tert-butyl acrylate) (PtBA) with associated roughness. We studied the effect of varying second stage monomer, co-swelling agent, and initiator on the size distribution of patches and particle surface roughness before and after sacrificial removal of patch domains. Sacrificial dissolution of PtBA domains by acid catalyzed hydrolysis (ACH) create chemically homogeneous dimpled particles with increased roughness than their patchy precursors. Depending on the diameter of the precursor PtBA patches, the dimpled particles are categorized as having golf-ball like/porous and multi cavity morphology. The underlying generality of the synthesis protocol allows for the surface features to be translated to varying particles sizes. Finally, because of the noncross-linked nature of the seed LPS, these surface anisotropic spherical particles were able to be stretched to ellipsoids, thus creating particles with both shape anisotropy and surface heterogeneity (chemical and topographical).

2. Materials and methods

2.1. Materials

The following chemicals were used as received without further purification: styrene (Sigma-Aldrich, 99%), poly(vinylpyrrolidone) (PVP, Sigma-Aldrich, 40,000 g/mole), Azobisisobutyronitrile (AIBN, Sigma-Aldrich, 99%), isopropyl alcohol (IPA, Fisher Scientific, Certified ACS, ≥ 99.5%), ethanol (EtOH, Fisher Scientific, Certified ACS, 95%) *tert*-butyl acrylate (tBA, Aldrich, 98%), 2,2′-azobis(2,4-dimethylvaleronitrile) (Wako V-65, >95%), poly(vinyl alcohol) (PVA, Sigma-Aldrich, 13,000–23,000 g/mole, 87–89% hydrolyzed), toluene (Fisher Scientific, Certified ACS, HPLC grade), trifluoroacetic acid (TFA, Sigma-Aldrich, 99%), gellan gum (GG, Thermo Scientific), Sylgard 184

curable silicone elastomer (poly(dimethylsiloxane) (PDMS), Dow Chemical Company). Ultrapure deionized water (DI, resistivity > 18.2 M Ω -cm, Millipore Milli-Q) was used for aqueous solution preparation and particle washing.

2.2. Synthesis of linear polystyrene (LPS) seed microspheres

LPS seed particles were synthesized via dispersion polymerization where 0.36 g PVP was added to 18.4 mL IPA in a 50 mL round bottom flask (RBF). In a separate glass vial, 0.05 g of oil soluble initiator, AIBN, was dissolved in 5.6 mL of styrene monomer and the resulting solution was added to the RBF. The solution in the RBF was purged with nitrogen for 5 min and then rotated in a 70 $^{\circ}$ C oil bath for 24 h to ensure complete polymerization. After polymerization, the particles were washed thoroughly with DI water by alternating centrifugation and sonication.

2.3. General procedure for synthesis of patchy spheres by seeded emulsion polymerization (SEP)

The general procedure of patchy microspheres fabrication involves a monomer mixture where 0.2 mL of tBA monomer was mixed with 0.5 wt % of V-65 initiator in a 7.1 mL glass vial. Next, 3.2 mL of 1 wt% aqueous PVA solution was added to the monomer mixture followed by vortexing for 60 s to form an emulsion. Afterwards, 0.3 g LPS seed spheres were added to the monomer emulsion vial that was then rotated at 30 rpm for 24 h to facilitate the swelling of the seed spheres with the monomer mixture. Subsequently, polymerization was performed by tumbling the seeded emulsion in a 70 °C oil bath at 40 rpm for 24 h. Finally, the product was harvested by washing with DI water by alternating centrifugation and sonication for at least six times. When the synthesis involved toluene as a co-swelling agent, the same procedure was followed except the addition of the desired volume of toluene after the addition of LPS seeds to the monomer emulsion and the removal of toluene before particle harvesting. Toluene was evaporated by removing the vial cap and maintaining 70 \pm 5 $^{\circ}$ C in the oil bath while stirring at 150 rpm. Experiments were carried out at varying polymerization conditions such as second-stage monomer (tBA), co-swelling agent (toluene), initiator loading, and reaction temperature following the same procedure. All experiments were conducted at least twice.

2.4. Stretching of microspheres to microellipsoids

Polymer microspheres were stretched into microellipsoids using an established method [27]. Briefly, the patchy microspheres were spread on a PVA solution held on a Teflon template and was allowed to dry. The dried thin film had a thickness of ~200 μm and was heated in an oil bath to a temperature of $T=115\,^{\circ}\text{C}$, which is above the glass transition temperatures, T_g , of all polymers (T_g , PtBA = 45 °C, T_g , PS = 107 °C, T_g , PVA = 75 °C) present in the film. The heated film was stretched to a predetermined draw ratio (2:1) to obtain particles with aspect ratio of 4. The stretched PVA film was then dissolved in water to recover the particles followed by at least six consecutive centrifugation-resuspension processes.

2.5. Selective dissolution of PtBA patch domains

To remove the patch (PtBA) domains from the PS-PtBA patchy microspheres and microellipsoids, ACH was done using TFA to convert PtBA domains into water-soluble poly(acrylic acid) domains, which were subsequently washed away with water. 3 mL of TFA was added to a glass vial containing 100 mg of PS-PtBA particles and was placed under magnetic stirring to facilitate the dissolution process. After 24 h of stirring, the particles were washed by alternating centrifugation and sonication. All of the subsequent washes were performed using DI water except the first one where EtOH was used to adjust the continuous phase density.

2.6. Particle characterization

Scanning electron microscopy (SEM) images were obtained using an FEI Magellan 400 XHR scanning electron microscope operating at acceleration voltage of 1 kV. The SEM samples were prepared via drop casting the particle suspension in water onto silicon wafer chips followed by drying at ambient conditions. The particles were imaged without a conductive metal coating. Using ImageJ, the diameters of the particles were measured by analyzing SEM images of>100 particles. The patch diameter was determined by measuring at least 200 patches spread across no less than 10 particles.

For chemical characterization of the produced particles before and after ACH, Fourier-transform infrared (FTIR) spectroscopy was done. FTIR spectra were recorded on a Spectrum One FTIR spectrometer (Universal ATR sampling accessory, PerkinElmer) in attenuated total reflectance (ATR) mode with a diamond crystal in the range of 4000–400 ${\rm cm}^{-1}$. To estimate the composition of the patchy colloids, thermogravimetric analysis (TGA) was performed on a TA Q500 thermogravimetric analyzer from 25 °C to 600 °C at a heating rate of 10 °C/min under a nitrogen atmosphere.

The surface roughness of the produced particles was measured by scanning a single particle via atomic force microscopy (AFM). Prior to AFM, the particles were immobilized on a PDMS film using gel trapping technique (GTT) [84]. In brief, a 2 wt% suspension of GG was prepared by adding the required amount of GG powder to DI water at 80 °C under continuous stirring at 1200 rpm for 2 h. 5 mL of 0.1 wt% particle suspension in water/EtOH (equal volume) were spread at the air-GG interface prepared by pouring GG solution into a 35 mm glass Petri dish. The addition of EtOH to the particle dispersions favors the interfacial spreading of particles driven by a Marangoni flow [85]. The samples were allowed to cool down to room temperature to jellify the aqueous GG phase and thus trap the particles at the interface. The PDMS was manually mixed with the curing agent in a 10:1 ratio and centrifuged at 4000 rpm for 15 min to remove all the gas bubbles that evolved from the mixing. Next, the gelled aqueous phase was carefully covered by PDMS elastomer and allowed to cure for 48 h at room temperature. The PDMS film containing the trapped particles was washed several times in DI water to remove any remining GG from the particle surface. Root-mean-square (RMS) roughness of the trapped particles was measured via AFM imaging on a single particle using an Asylum MFP-3D. Tapping mode images were acquired via probing the sample surface with an Olympus AC240TS-R3 silicon cantilever having a spring constant of 2 Nm⁻¹ and a resonance frequency of 70 kHz at ambient

condition. The open-source software Gwyddion [86] was used to analyze the obtained images. To obtain RMS values, the macroscopic particle curvature was subtracted to obtain the residual surface height profile, from which the RMS roughness was calculated. The RMS values and its standard deviation were calculated from a minimum of two regions measuring 1.5 μm by 1.5 μm area each, spanning over more than five particles.

3. Results and discussion

3.1. Tuning patchiness and chemical anisotropy in microspheres

The chemical and physical surface heterogeneity of colloids can be tuned by numerous process parameters in SEP, and in particular the effects of monomer, co-solvent, and initiator concentration are focused on here. The dispersion polymerization of styrene in IPA reaction medium in the presence of PVP polymeric stabilizer yields $4.14 \pm 0.12~\mu m$ diameter non-crosslinked LPS spheres with low polydispersity and high reproducibility (the corresponding SEM image along with the diameter distribution is shown in Figure S1). These particles serve as seeds for the subsequent SEP technique used to fabricate patchy rough spherical colloids. Fig. 1 depicts the synthetic path followed to fabricate patchy rough microspheres, where both chemical and physical surface heterogeneity are integrated. The LPS seed particles are swollen with a mixture of hydrophobic monomer and initiator, tBA and V-65, respectively, for 24 h and emulsified in an aqueous environment containing 1 wt% PVA stabilizer. We define the amount of second-stage monomer (tBA) introduced into the reaction system to be the volume of monomer added to the total volume of monomer and seed, or $\emptyset = \frac{V_{BA}}{V_{RA} + V_{seed}}$, and the amount of initiator, I, to be wt% of the initiator based on the added tBA. Upon completion of the swelling period, the system containing the seeded emulsion droplets were heated up to a temperature (T) of 70°C to trigger the polymerization of tBA and kept for 24 h to ensure complete conversion [87]. Since the seed spheres are swollen with tBA monomer, polymerization occurs at nucleation sites which cause the growth of phase separated PtBA domains within the continuous LPS phase due to the incompatibility of the two polymer phases, [88] which is known as PIPS [15].

A value of $\emptyset = 0.4$ and I = 0.5 wt % was chosen as the model system for investigation since the previous work by Hamilton *et al* [87] reported a transition from patchy-Janus to patchy morphology at this reaction condition, however, prior work used different sized seed spheres with

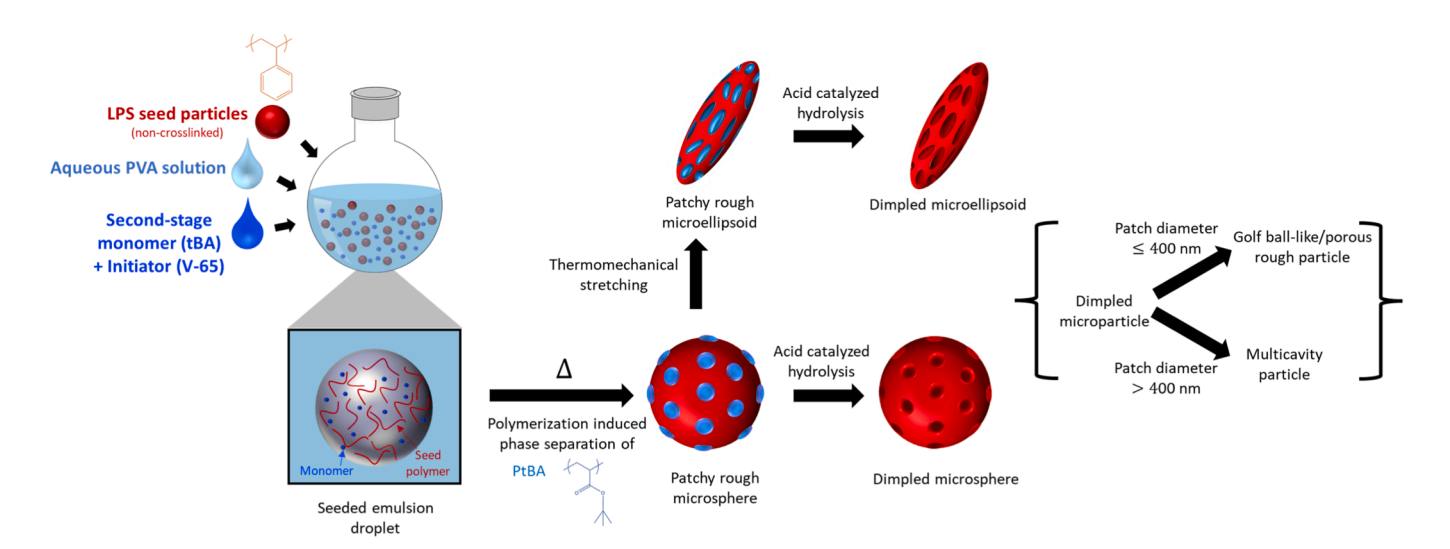


Fig. 1. Schematic illustration of the preparation route for patchy rough and dimpled (golf-ball like/porous rough and multicavity) microspheres and microellipsoids.

different surface chemistry. Fig. 2 demonstrates the morphology and patch diameter distribution of the achieved microspheres. It is obvious that the microspheres possess a patchy morphology as evident from the circular patch domains that are visible by SEM. This appearance is due in part to the electron beam damage of the PtBA [87], and as discussed later also a result of roughness on the surface of the particle. The average diameter of the patches is $0.20 \pm 0.06 \, \mu m$. Such small patch domains are the result of incomplete phase separation of PtBA from the LPS phase that renders the system to be in a thermodynamically unstable state [15]. Due to the incorporation of the PtBA in the SEP process, the particle diameter increased by 12% which gave an average particle diameter of 4.60 \pm 0.12 μm with a coefficient of variation (CV) of 2.6%. This polydispersity is similar to the seed spheres, indicating the robustness of the SEP process. Therefore, the SEP technique applied to this reaction chemistry can produce microspheres with homogeneous nanoscale surface patches. Expanding upon this result, we opted to tune the morphology of the patchy microparticle by varying the reaction parameters, in particular, the amount of second-stage monomer (Ø) and wt % of initiator (I) introduced, adding toluene as a co-swelling agent, and the reaction temperature (T).

The surface morphology of the patchy microspheres can be altered by varying the amount of second-stage monomer-tBA (\varnothing) as shown in Fig. 3. From SEM images (Fig. 3a), it is obvious that some of the patch domains remain circular and become larger by increasing the value of \varnothing from 0.4 to 0.8. The surface morphology is characterized in different ways, including the box plot of patch diameter (Fig. 3b), and the patch area distribution (Fig. 3c). The corresponding histograms are shown in Figure S2a. While the the largest patch diameter increases with the increase in \varnothing , the average diameter only increases slightly and minimum patch diameter remains at the same value. The number distribution of patches becomes somewhat bidisperse, as smaller patches remain between the larger patches. As \varnothing increases, fewer, larger patches are present, however these patches dominate the surface of the particle on an areal basis (Fig. 3c).

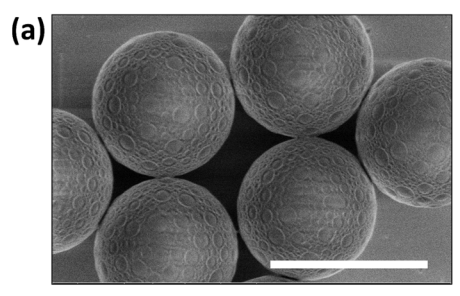
With the increase of Ø, the amount of tBA absorbed in the seed increases during the swelling stage which reduces the viscosity of the seeded droplet, enhancing the mobility of the formed PtBA polymer molecules to coalesce into larger domains. In addition, upon polymerization, the PtBA domains preferentially absorb the remaining tBA monomer as well as any formed oligomers in the reaction system to grow into larger domains as a way of minimizing the total interfacial tension [89], with larger sized domains having higher affinity for tBA absorption. These two factors-viscosity reduction and monomer absorptioninduced domain augmentation dictate the final particle surface morphology. As Ø is increased from 0.4 to 0.6, the viscosity decreases while monomer absorption increases, collectively contributing to an increased average patch diameter and polydispersity. Therefore, some PtBA domains grow into larger domains due to phase coalescence and some domains grow even larger due to enhanced absorption of tBA. However, further increasing the \emptyset to 0.8, the average dimeter as well as the box range decreased as the domain growth was highly influenced by

the monomer absorption at this high tBA concentration. The polymerization of tBA proceeds much faster in the already formed PtBA domains than in the LPS bare surface, resulting in rapid enlargement of the PtBA domains [90]. Moreover, the PtBA domains seem to protrude slightly from the continuous LPS phase as \varnothing increases in an attempt to minimize the surface area between two incompatible polymer phases. These conclusions are reinforced by observing the cumulative frequency (f) of the patch domains (Figure S3a) where the frequency graph for $\varnothing=0.5$ and 0.6 coincides with that of 0.4 until a value of f=0.75 and 0.6 is reached for $\varnothing=0.5$ and 0.6, respectively. However, for $\varnothing=0.8$, the frequency distribution deviated from that of $\varnothing=0.4$ at a value of f=0.85, again showing a small population of larger patches that dominate the surface of the particle (Fig. 3c).

Most often the ultimate material properties that are derived from the patchy particles depend significantly on the patch area. As a result, the influence of \varnothing on the area distribution of the patches was analyzed (Fig. 3c). We divided the patch areas into three regions: $\le 0.1~\mu\text{m}^2$, $>0.1~\text{and} \le 1~\mu\text{m}^2$, and $> 1~\mu\text{m}^2$. Specifically, when \varnothing is at its lowest value of 0.4, the patches are $\le 0.1~\mu\text{m}^2$. When \varnothing increases, even though the number of small patches remains significant (as seen in Fig. 3b), the surface area of the particle becomes increasingly dominated by the small number of large patches. For example, when \varnothing is at its highest value of 0.8 only 3% of the total patch area is $\le 0.1~\mu\text{m}^2$ while over 90% of the patch area comes from large (>1 μm^2) patches, despite having a similar average patch diameter.

To quantify the amount of PtBA incorporated into the microsphere, TGA was done on the synthesized patchy particles that shows a positive correlation with increasing \varnothing (as reported in Table S1), as expected from the increased amount of monomer added. This can also be confirmed from the escalating increase in particle diameter as \varnothing rises (as reported in Table S1). The yield of PtBA remains almost same as a function of \varnothing (from 0.4 to 0.8) as shown in Figure S4a. We note that SEP performed at $\varnothing=0.2$ resulted in visually homogeneous spheres and no PtBA was found in the particles. This indicates that there must be a minimum amount of tBA should be present in the seeded emulsion system to provide enough driving force for swelling of the seed spheres with tBA that upon polymerization transform into PtBA domains.

Based on these results, we hypothesized that decreasing the viscosity of the seeded emulsion droplet would result in greater coalescence of PtBA domains during polymerization, generating particles with more homogeneous domains. To test this hypothesis, toluene was introduced as a non-polymerizable co-swelling agent and varied systematically to observe its influence on final particle surface morphology. The amount of toluene introduced into the reaction system is defined as the ratio of volume of toluene added to the volume of monomer or $\tau = \frac{V_{olluene}}{V_{UBA}}$. Fig. 4a demonstrates the SEM images of patchy microspheres produced with $\varnothing = 0.4$ and 0.5 and τ varying from 0 to 1. It is evident from the SEM images that smaller domains disappear and larger domains appear as τ increases, which is quantified in the box plot (Fig. 5a) of the patch diameters (corresponding histograms are shown in Figure S2b). In contrast



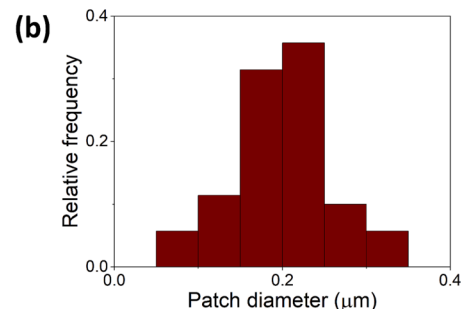


Fig. 2. (a) SEM image of particle morphology and (b) patch size distribution of patchy microspheres prepared from PIPS of PtBA domains on LPS continuous phase ($\emptyset = 0.4$). Scale bars represent 5 μ m.

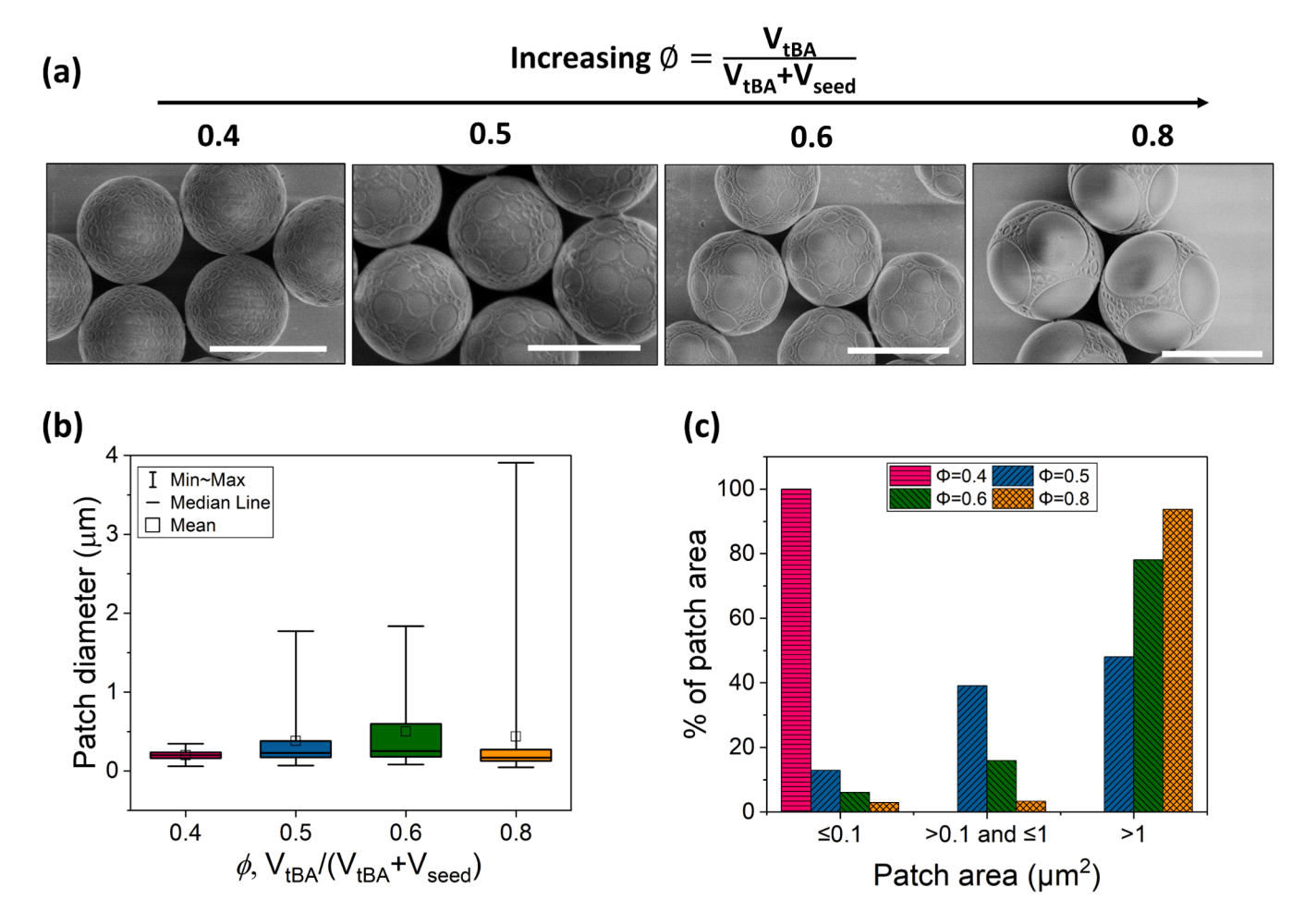


Fig. 3. Controlling the morphology of patchy spheres with addition of second-stage monomer (\emptyset). (a) SEM images, (b) box plot of patch size distribution, and (c) area distribution of patches. Scale bars represent 5 μ m.

to what was observed with increasing Ø, the average and minimum patch diameter both increase notably. As a good plasticizer, toluene swells the LPS continuous phase and reduces the viscosity of the colloidal interior [91]. The decrease in the viscosity enhances the mobility of the growing PtBA polymer chains/domains, and hence, increasing the rate of domain coalescence to decrease the interfacial area between the two mismatched polymer phases. Therefore, more and more smaller domains coalesce as τ increases to increase the minimum patch diameter in the box plot. This is also obvious from the f plot of the patch domains (Figure S3b) where the frequency data moves to the right spanning over all the possible patch diameters. This means that the probability of combining smaller patch domains surge with increasing toluene that drives the system towards attaining more homogeneous patch sizes. Therefore, with added toluene, the viscosity induced domain coalescence is the main contributing factor for domain enlargement as opposed to what observed with high Ø. As expected, the particle surface is dominated by larger patches with increasing τ (Fig. 5b). However, while changing second stage monomer concentration results in particles dominated by either small or large patch areas, introducing intermediate amounts of toluene is able to more continuously tune the patch diameter, enabling production of particles with the majority of patch areas coming from intermediate sized patches (>0.1 and $< 1 \mu m^2$). With varying τ, the % yield of PtBA as obtained from the TGA analysis (Figure S4b) remains constant and similar to the yield measured in the absence of toluene. This rules out the possibility of competition between tBA and toluene absorption by the seed LPS, which would decrease the amount of PtBA in the final particle. Overall, adding a co-swelling agent or plasticizer has significant impact on the patch morphology and a

similar behavior is also expected for other values of Ø.

In order to modulate the morphology of microparticle via controlling the reaction kinetics, we systematically investigated the effect of initiator on the particle morphology. The wt% of initiator (*I*) was varied from the standard value of 0.5 wt% with $\emptyset = 0.4$ and 0.5, and the obtained SEM images are shown in Fig. 4b. In general, smaller, more homogeneous patches resulted as I increased. The average patch diameter decreased from $0.20 \pm 0.06~\mu m$ to $0.12 \pm 0.04~\mu m$ when the I was increased from 0.5 wt% to 2.5 wt% for $\emptyset = 0.4$. Particles with $\emptyset = 0.5$ also behaved in a similar way since the average diameter and the range between minimum and maximum patch diameter decreases as well as the area contribution from patches $\leq 0.1 \, \mu \text{m}^2$ increases with increasing I, as shown in Fig. 5c-d. The reason for decreased patch size can be attributed to the change in reaction rate that also comes into play along with the previously discussed viscosity induced domain migration and merging. Increased I induces a larger number of radical nucleation sites contributing to an increase in the polymerization rate that outweighs the domain coalescence rate. This serves to accelerate the phase separation and results in smaller and more homogeneous patch domains. However, the monomer absorption by the already formed PtBA domains was not impacted by the changing *I* as the % yield of PtBA as well as the amount of PtBA incorporated in the microsphere obtained from TGA remained unchanged, as shown in Figure S4c. Interestingly, the particles didn't show any patchiness when the I was decreased to 0.1, indicating that a minimum amount of initiator is required for the tBA oligomers to grow to a critical chain length so phase separation from the continuous LPS phase can occur. This is confirmed by TGA as no PtBA was found in the resultant particles at this low initiator concentration (Figure S4c).

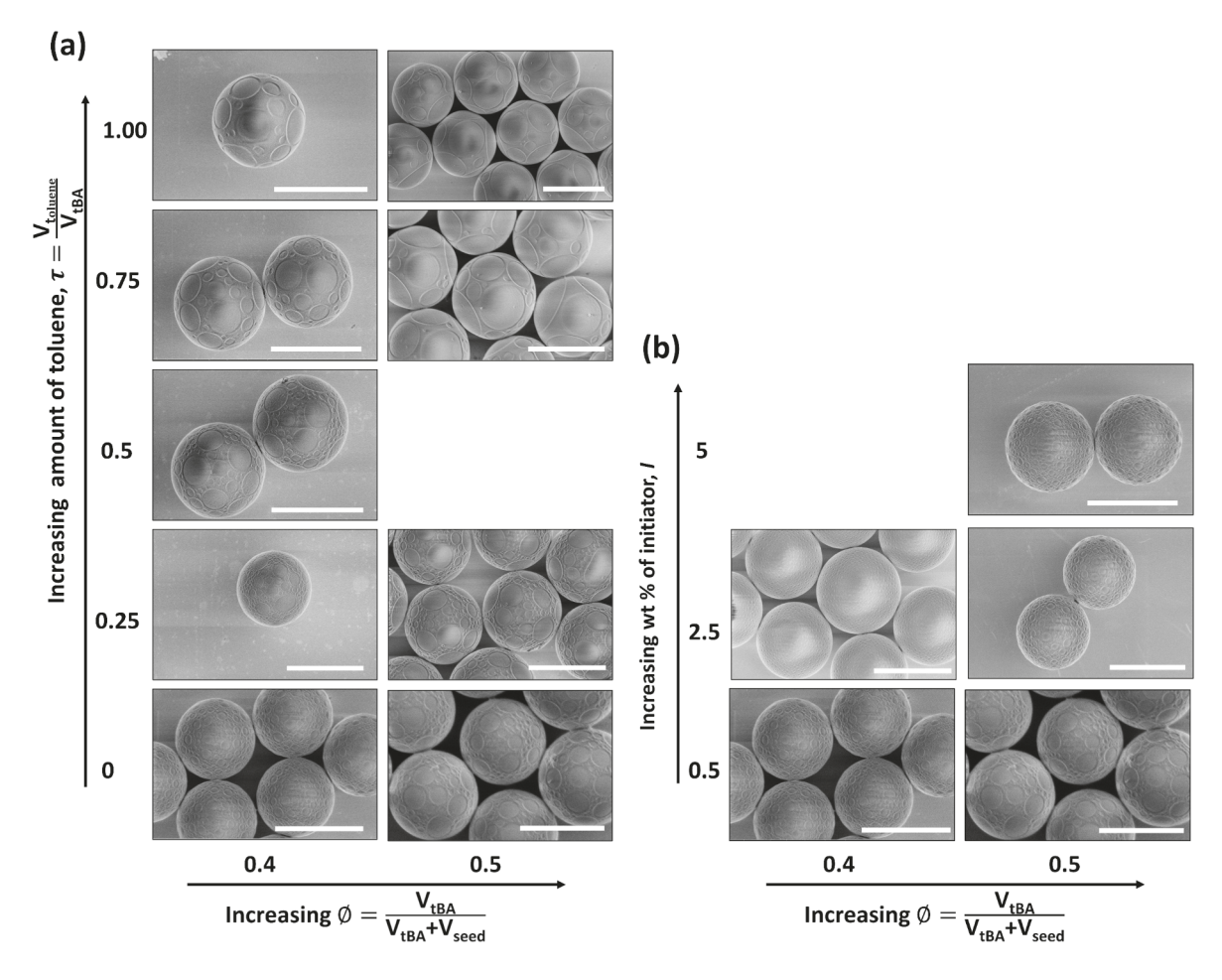


Fig. 4. SEM images of patchy spheres synthesized using varying amount of (a) toluene (τ) and (b) initiator (I) for Ø = 0.4 and 0.5. Scale bars represent 5 μm.

Lastly, we attempted to change the morphology of the resulting microspheres by adjusting the reaction temperature (T). The SEM images of the particle surface ($\emptyset = 0.4$ and 0.5) captured at various T are displayed in Figure S5. At a lower T (55°C), particles with $\emptyset = 0.4$ exhibited no well-defined patches. It is likely at this low T, the radical formation rate was reduced sufficiently enough, along with the low amount of tBA added, that the growing oligomeric radicals did not reach a critical value required for phase separated domain formation and the subsequent monomer absorption. However, for particles derived from higher tBA concentration ($\emptyset = 0.5$), precise domain formation occurred as now more tBA monomers are available for the oligomeric radicals to reach the critical length for domain formation despite this lower polymerization rate. In addition, at reduced T the viscosity is also increased, resulting in lowered domain amalgamation and more homogeneous surface features. When the T was increased to 85°C, the domain size and areal density decreased and increased, respectively, on account of dominating reaction rate over domain migration and fusion rate induced by the reduced viscosity at higher T. This also helped in narrowing the distribution of patch sizes. At the standard temperature of 70°C, both the reaction propagation rate and the domain consolidation rate were comparable, while the post domain monomer absorption was responsible for larger patch domains as observed for higher tBA content (\emptyset = 0.5).

The above findings indicate that altering monomer concentration, adding co-swelling agent, and changing initiator amount and reaction temperature are efficient means of adjusting the size and surface patterning of polystyrene microspheres with patchy or chemically inhomogeneous PtBA surface features. Next, we show that this chemical inhomogeneity is linked to surface topographical inhomogeneity and

show how subsequent modification of these particles produces porous particles with controlled surface roughness in both spherical and ellipsoidal particles.

3.2. Tuning roughness and multicavity anisotropy

Based on the SEP described above, in general two types of patchy spheres are produced: those with small ($\leq 0.1\,\mu\text{m}^2$ area or 400 nm diameter), uniform patches, and those with large or polydisperse patches. We refer to the prior group as "rough spheres", and the latter as "multicavity particles", due to the morphology of the particle after ACH, which is described here. Prior to ACH, the rough spheres maintain an overall spherical shape and appear slightly dimpled, reflecting a rough texture. As discussed below, the appearance of patchiness under SEM is indeed due to surface roughness and not just an artifact of PtBA being damaged by the electron beam during imaging. As a result, these particles are similar to raspberry-like particles synthesized by other methods [23,78]. This region is interesting from a fundamental point of view, as there have been numerous recent studies on the effect of roughness on the bulk and interfacial suspension properties. Via this synthetic approach, controlled surface roughness is achieved mainly by modulating the wt% of initiator. This synthesis leads to a coupling between surface roughness and chemical heterogeneity, whereby the latter is directly related to surface patchiness. According to the definition of key AD prescribed by Glotzer and Solomon [32], these particles have AD

To decouple chemical and physical anisotropy, the patchy domains were removed by ACH that converts the PtBA domain into water soluble polyacrylic acid [87], which is water washed to result in chemically

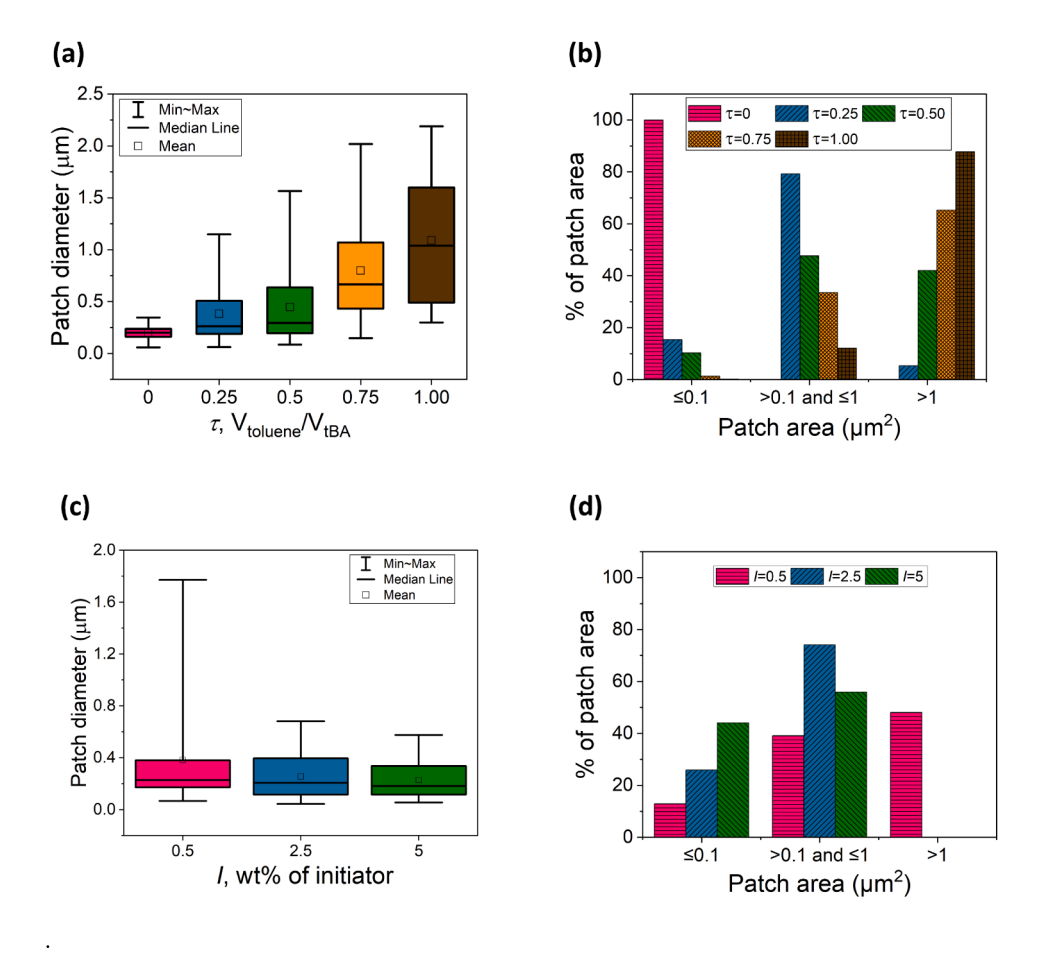


Fig. 5. Effect of toluene (τ) and initiator (I) on the morphology change of patchy spheres. Size and area distribution of patches at varying τ (a and b, \emptyset =0.4) and I (c and d, \emptyset =0.5).

homogeneous particles (AD = 1). The corresponding SEM images of post-ACH particles are shown in Fig. 6. The removal of PtBA was confirmed by FTIR analysis (see Figure S6 and associated SI text). TGA analysis (Figure S7) also confirms the expulsion of PtBA domain as the thermal decomposition of the microparticles after ACH occurs in a single step stage at around 400 °C, which is responsible for the decomposition of LPS, as opposed to two stages before ACH, the first of which is responsible for the decomposition of *tert*-butyl group at about 250 °C [92]. When performing ACH on the rough spheres with patchy, raspberry-like, morphology, the resultant particles resembled golf balls, with dimples that were closely correlated with the protrusions of their raspberry-like precursors. These golf-ball like/porous particles are marked by the red dotted box in Fig. 6.

The patchy particles which possessed large (> $0.1 \, \mu m^2$ area/400 nm diameter) or polydisperse domains, produced multicavity particles after ACH (Fig. 6, marked by green dotted box). Since the position and size of the created dimples are highly associated with the precursor patchy protrusions, the similar effect of modifying \emptyset and τ on patchy particles is reflected on the multicavity particles. As discussed earlier, with increasing Ø, some PtBA domains grow into larger domains due to enhanced absorption of tBA while there are still small domains present. Post removal of these domains show the same surface features with deeper dimples or cavities yielding from larger protrusions and vice versa. Finally, at $\emptyset = 0.8$, tetrahedron dimpled colloidal particles are observed. On the other hand, with increasing τ smaller domains disappear and larger domains appear, since the collision and merger between the PtBA domains are more likely due to the reduced viscosity of the LPS phase. Therefore, as τ increases, post-ACH particles show cavities growing deeper and larger while smaller ones disappear, and the overall number of cavities decrease. At a higher value of τ , it is expected that tetrahedron dimpled particles will appear, however, without any small pits obtained with higher \varnothing . These particles have the potential to form colloidal clusters with a well-defined complex structure through depletion interaction and centrifugal force driven assembly with well-matched spherical particles [24].

The RMS surface roughness of "rough spheres" before and after ACH was characterized by AFM. Fig. 7a presents the RMS roughness of the particles as a function of I at $\emptyset = 0.4$ and 0.5 before and after sacrificial dissolution of PtBA domains, with roughness values ranging from 3 nm to 44 nm found. Before ACH, as I increased from 0.5 to 2.5, the RMS roughness decreases for particle with $\emptyset = 0.4$, whereas for $\emptyset = 0.5$, the RMS roughness increases as I goes from 2.5 to 5. The roughness values of these raspberry-like particles are correlated mostly with the height of patch protrusions and, to some extent, the patch areal density [54]. In general, an increase in asperity height is associated with an increase in RMS roughness that comes along with decreased number of asperities per unit area and vice versa. However, a moderate surface patch elevation and intensity can also yield higher RMS roughness values. The relative contribution of these two opposite phenomena dictates the final surface roughness value. With the increase in initiator concentration, the asperity density increases (as the patch diameter decreases) while the asperity height decreases, to achieve more uniformity. Therefore, the increase in I yielded a decrease in RMS roughness in spheres with \emptyset = 0.4. However, for particles obtained from $\emptyset = 0.5$, an increase in *I* caused a rise in the roughness value since now the contribution from both asperity height and density to the final RMS roughness are comparable. The RMS roughness is therefore expected to diminish at even larger *I* as the patch protrusion height will decrease accompanied by an increase in

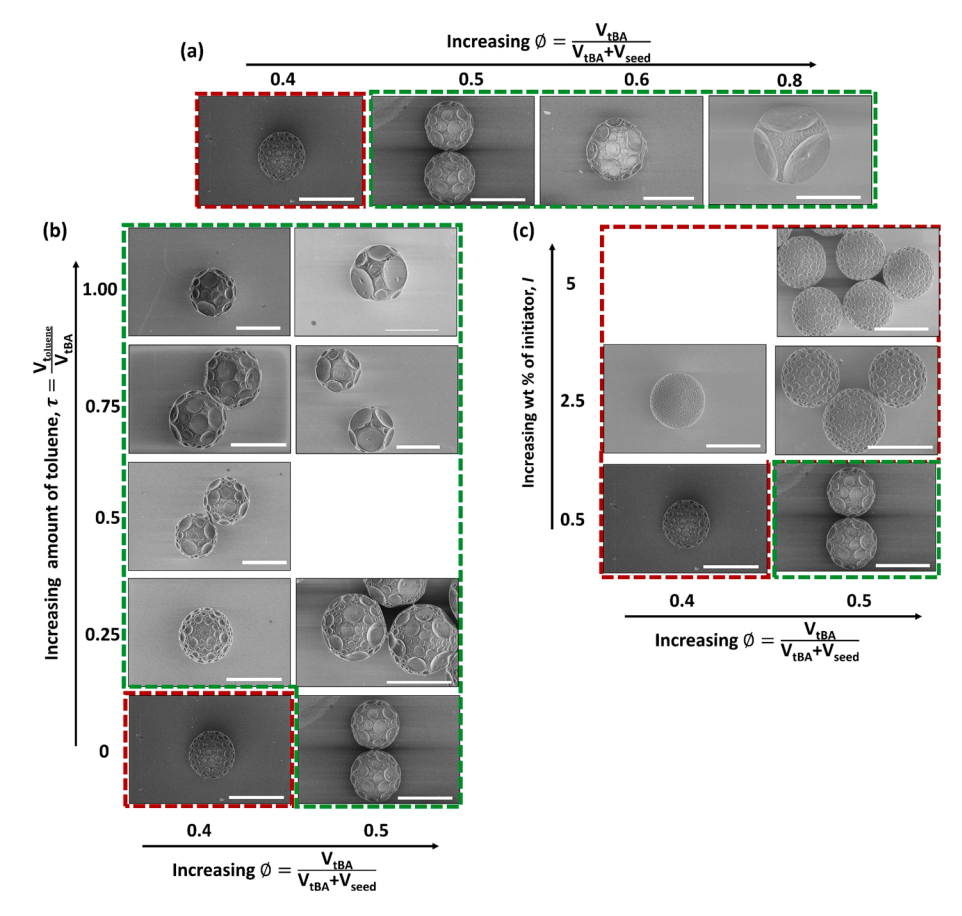


Fig. 6. SEM images of golf ball-like/porous (red dotted box) and multicavity (green dotted box) particles at varying amount of (a) second-stage monomer (\emptyset), (b) toluene (τ), and (c) initiator (I) obtained from ACH of patchy spheres. Scale bars represent 5 μ m. (For interpretation of the references to colour in this figure legend, the reader is referred to the web version of this article.)

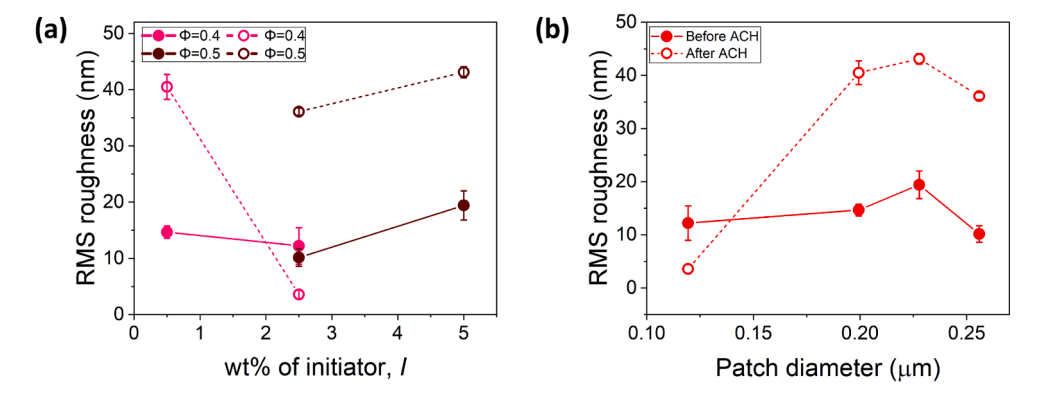


Fig. 7. The RMS roughness of spheres before and after ACH as a function of (a) reaction conditions and (b) original patch diameter. Solid symbol represents particles before ACH and hollow symbols represent particles after ACH.

surface patch density.

Another effective way to understand how particle roughness can be manipulated by this approach is to compare the change in RMS roughness with the patch diameter as reported in Fig. 7b. When the patch diameter is very low (0.12nm) the high patch areal density and low patch protrusion contributes to lower roughness value. As the patch diameter increases, the areal density decreases and the corresponding patch protrusion increases, which reflects an increase in RMS roughness. However, after a certain patch diameter (0.23nm), the decrease in areal density is no longer associated with the increase in patch protrusion because for a constant amount of \varnothing the patch will become flatter to

cover a larger area, shifting the roughness value to a lower value. This result means that an increase in roughness can be achieved via increasing \varnothing that will increase the patch protrusion and diameter. To increase roughness at constant patch diameter, I may be increased in conjunction with \varnothing . Therefore, careful selection of the SEP reaction conditions can result in particles with varying levels of roughness.

In general, following the ACH-enabled sacrificial dissolution of PtBA domains, the RMS roughness of the golf-ball like particles increased dramatically (Fig. 7a-b). These findings can be attributed to the deeper dimples produced from larger protrusions. For example, in Fig. 7a, for particles with $\varnothing=0.5$, the roughness values show a trend similar to that

was observed before ACH. The same reason supports the observed phenomena, i.e., a combined effect from dimple depth and density dictates the final surface property. At a lower concentration of initiator, roughness is dominated by dimple depth giving relatively lower RMS values and at a moderate concentration of initiator, both the surface penetration and number per unit area contribute to the higher roughness features. Although not investigated here, it is hypothesized that at even higher initiator loadings, the roughness value will dwindle as the high contributing factor-dimple depth will decrease and the low contributing factor-dimple density will increase. An exception to these trends is found with particles having \emptyset , I = 0.4, 2.5 chemistry. In this case, a high patch density resulted in a very low patch heights that produced shallow dimples, and the dimples depth were lower than the overall height of the precursor patches that resulted in lower RMS roughness than the precursor patchy particles. A similar behavior is also expected for $\emptyset = 0.5$ particles at a very high value of I. The same also holds true when the roughness values are compared with respect to patch diameter in Fig. 7b. While we have focused our systematic study using 4.1 μm diameter LPS seed particles, in SI Figure S8 and S9 we show how this approach can be successfully extended to seed particle diameters ranging from 1.3 to 4.6 µm. Interestingly, with the same reaction conditions the patch diameter increases only marginally with seed particle diameter, indicating the potential for orthogonal control of the overall particle and patch dimensions.

These results demonstrates a facile way of synthesizing both chemically inhomogeneous (rough, raspberry-like particles) and homogeneous (porous, golf ball-like) spheres, where the former can be used as precursors to fabricate and tune the latter microparticles. In the following section, we describe the use of the pre-ACH particles to translate these interesting topological and chemical anisotropy dimensions to ellipsoids.

3.3. Translation of surface features to ellipsoids

Shape anisotropic particles, such as ellipsoidal particles, with patchy or raspberry-like surface features have barely been reported previously. This is because often the patchiness and/or roughness cannot directly be translated from spherical to shape anisotropic particles and can only be introduced on post synthesized particles [12]. With our synthesis protocol, the surface features of spherical particles can be easily translated to ellipsoidal particles. Patchy microspheres are made of uncrosslinked LPS seeds, which are easily transformed into ellipsoids with the desired aspect ratios by thermomechanical stretching at a temperature greater than the T_g of both PtBA and PS polymers. As shown here, this process also retains the surface characteristics discussed above for spherical particles. Like patchy spheres, patchy ellipsoids can undergo ACH to eliminate the PtBA domains. Fig. 8 shows SEM images before and after ACH of ellipsoids having aspect ratio of 4 obtained from the stretching of

selected patchy particles corresponding to the "rough spheres" (marked by red dotted box in Fig. 6) and multicavity particles (marked by green dotted box in Fig. 6). Irrespective of the sample, it is obvious from the SEM images that the surface patchiness nicely translates into the ellipsoids. The stretched patches maintain the same aspect ratio as the ellipsoids, according to the AFM images (Figure S10). Having introduced aspect ratio induced anisotropy, the AD of obtained ellipsoids is 3 (particle shape, roughness, chemical heterogeneity) and 2 (particle shape, roughness), before and after ACH, respectively. AFM was performed on the ellipsoids formed from the spheres analyzed in Fig. 7a-b, with the results shown in Fig. 9a-b. It is obvious that the RMS roughness follows the same trend as for the spheres, with the roughness values dramatically increasing after removal of PtBA domains. When compared to the patchy rough spheres before ACH (Fig. 9b), the patchy rough ellipsoids show lower roughness values than their spherical counterparts. This could be due to microsphere stretching causing the patch protrusion height to decrease, which is positively connected with the RMS roughness values. However, after ACH, the roughness of porous microellipsoids remains the same or slightly increases as shown in Fig. 9b. Stretching appears to have less impact on the dimple depth than it does on the precursor asperity height, which decreases as the particle is stretched. This finding not only demonstrates that the surface heterogeneities, whether chemical or physical, can successfully be transferred into shape anisotropic particles but emphasizes the potential of adjusting the surface heterogeneities by tuning the morphologies of the spherical seed particles.

4. Conclusions

In summary, we presented a facile method based on SEP to create PS microspheres and microellipsoids with varying surface patches of PtBA. Whereas prior work incorporated patchiness or roughness to spherical particles [23,74,78], or to ellipsoids [80-83] separately, here we develop a unified approach to make complementary spheres and ellipsoids with controlled surface topography and chemistry. By selecting synthesis conditions to avoid crosslinking of polymers and by choosing comonomer chemistry carefully, we successfully translated surface features into microellipsoids and selectively removed patch regions, producing particles with multidimensional anisotropy ranging from AD = 1 - 3. LPS seed mediated emulsion polymerization of a second monomer (tBA) formed patchy or raspberry-like particles. The patch diameters and protrusions were well controlled by adjusting the polymerization parameters such as monomer concentration, co-swelling agent/plasticizer (toluene), initiator loading, and reaction temperature. The size, areal density, and height of the patches was attributed to the balance between two competing factors: domain coalescence from reduced viscosity in the seeded droplets and domain growth due to monomer absorption by already formed domains. To decouple the

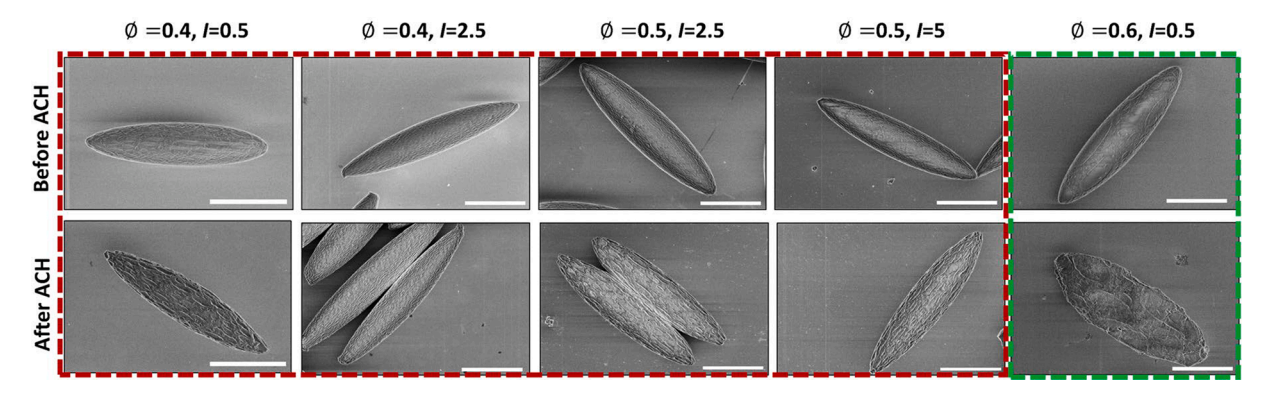


Fig. 8. SEM images showing translation of surface patchiness to microellipsoids obtained from stretching of different patchy spheres. Red dotted box and green dotted box indicate particles coming from spheres having patch domain diameters \leq 400 nm and > 400 nm, respectively. Scale bars represent 5 μ m. (For interpretation of the references to colour in this figure legend, the reader is referred to the web version of this article.)

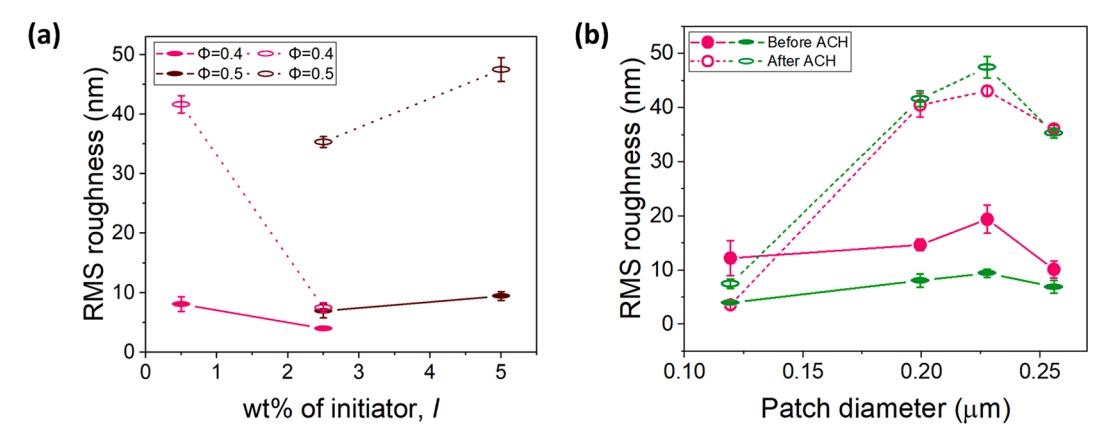


Fig. 9. The RMS roughness of (a) ellipsoids before and after ACH and (b) spheres and ellipsoids as a function of original patch diameter. Solid symbol represents particles before ACH and hollow symbols represent particles after ACH, with the given initiator (I) and secondary monomer concentration (\varnothing).

chemical anisotropy from roughness, ACH was used to remove the PtBA patch domains, leaving dimples on the continuous LPS matrix and increasing the roughness further. ACH of particles with large patch domains gave rise to faceted tetrahedron dimpled particles, while ACH of particles with small homogeneous domains resulted in porous, golf-ball like particles. The non-crosslinked nature of the seed spheres allows the microspheres to transform into microellipsoids via thermomechanical stretching while retaining their surface features, be it patchiness, roughness, or facets. Overall, in this synthesis technique we can achieve microparticles with several key anisotropy dimensions [32] - patchiness, roughness, and faceting-that can be scaled in different particle sizes while maintaining a high yield. In addition, these anisotropy dimensions can easily be integrated into ellipsoids with different aspect ratios - another anisotropy dimension - yielding particles with multidimensional anisotropy. While this work has been focused on using PtBA as the co-monomer with PS seed spheres, we expect that it will be generalizable to many combinations of seed particles and monomers. For example, preliminary experiments we have carried out with butyl acrylate, propargyl acrylate, benzyl acrylate as comonomers have shown promising results. Moreover, the possibility of swelling seeds with multiple comonomers to create patchy particles with well-defined chemical regions can be realized via this technique [87]. However, it is crucial to carefully consider various factors, including the Tg and the miscibility of the swelling monomer with the seed polymer, which we expect to also impact the details of the resultant particle morphology. Overall, this SEP based approach has the potential to lend a complementary handle to tune the interfacial interaction and rheology of particle laden interfaces via introducing surface patches and/or roughness, enabling the creation of innovative functional materials with enhanced properties.

CRediT authorship contribution statement

Md Anisur Rahman: Methodology, Formal analysis, Investigation, Writing – original draft, Writing – review & editing, Visualization. Taina Turner: Formal analysis, Investigation. Heather.S.C. Hamilton: Investigation, Methodology, Resources, Writing – review & editing. Laura C. Bradley: Conceptualization, Resources, Writing – review & editing. Peter J. Beltramo: Conceptualization, Funding acquisition, Project administration, Supervision, Writing – original draft, Writing – review & editing.

Declaration of Competing Interest

The authors declare that they have no known competing financial interests or personal relationships that could have appeared to influence the work reported in this paper.

Data availability

Data will be made available on request.

Acknowledgements

We acknowledge funding for this research provided by the National Science Foundation under award no. CBET-2232579 and as well as support from the ASCENDS REU program (T.T.). Colloid characterization was performed at the UMass Amherst Center for Electron Microscopy, and the authors thank Dr. Alexander Ribbe for assistance with SEM and AFM.

Appendix A. Supplementary data

Supplementary data to this article can be found online at https://doi.org/10.1016/j.jcis.2023.08.083.

References

- [1] Z. Zhang, S.C. Glotzer, Self-assembly of patchy particles, Nano Letters 4 (2004) 1407–1413, https://doi.org/10.1021/nl0493500.
- [2] E.W. Edwards, D. Wang, H. Möhwald, Hierarchical organization of colloidal particles: From colloidal crystallization to supraparticle chemistry, Macromol Chemical Physics 208 (2007) 439–445, https://doi.org/10.1002/ macr. 2006.006.55
- [3] S.C. Glotzer, M.J. Solomon, N.A. Kotov, Self-assembly: From nanoscale to microscale colloids, AIChE Journal. 50 (2004) 2978–2985, https://doi.org/ 10.1002/aic.10413
- [4] E.Y.K. Fung, K. Muangnapoh, C.M. Liddell Watson, Anisotropic photonic crystal building blocks: colloids tuned from mushroom-caps to dimers, Journal of Materials Chemistry 22 (2012) 10507–10513, https://doi.org/10.1039/ C2.10001.208
- [5] E.K. Riley, E.Y. Fung, C.M.L. Watson, Buckled colloidal crystals with nonspherical bases for two-dimensional slab photonic band gaps, Journal of Applied Physics 111 (2012) 093504, https://doi.org/10.1063/1.4706556.
- [6] J.D. Forster, J.G. Park, M. Mittal, H. Noh, C.F. Schreck, C.S. O'Hern, H. Cao, E. M. Furst, E.R. Dufresne, Assembly of optical-scale dumbbells into dense photonic crystals, ACS Nano 5 (2011) 6695–6700, https://doi.org/10.1021/NN202227F/SUPPL.FILE.NN202227F SI 005. AVI.
- [7] E. Hinde, K. Thammasiraphop, H.T.T. Duong, J. Yeow, B. Karagoz, C. Boyer, J. J. Gooding, K. Gaus, Pair correlation microscopy reveals the role of nanoparticle shape in intracellular transport and site of drug release, Nature Nanotechnology 12 (2017) 81–89, https://doi.org/10.1038/NNANO.2016.160.
- [8] D.H. Kim, H.-C. Woo, M.H. Kim, Room-temperature synthesis of hollow polymer microparticles with an open hole on the surface and their application, Langmuir 35 (2019) 13700–13710. https://doi.org/10.1021/acs.langmuir.9b02780.
- [9] W. Gao, A. Pei, R. Dong, J. Wang, Catalytic iridium-based janus micromotors powered by ultralow levels of chemical fuels, Journal of the American Chemical Society 136 (2014) 2276–2279. https://doi.org/10.1021/ja413002e.
- [10] K.C. Bryson, T.I. Löbling, A.H.E. Müller, T.P. Russell, R.C. Hayward, Using janus nanoparticles to trap polymer blend morphologies during solvent-evaporationinduced demixing, Macromolecules 48 (2015) 4220–4227, https://doi.org/ 10.1021/acs.macromol.5b00640.
- [11] S. Samanta, S.L. Banerjee, S.K. Ghosh, N.K. Singha, Smart polyacrylate emulsion based on a new ABC-type triblock copolymer via RAFT-mediated surfactant-free

- miniemulsion polymerization: its multifunctional properties, ACS Applied Materials & Interfaces 11 (2019) 44722–44734, https://doi.org/10.1021/accepti_0b15064
- [12] P. Zhang, L. Yang, Q. Li, S. Wu, S. Jia, Z. Li, Z. Zhang, L. Shi, Ellipsoidal colloids with a controlled surface roughness via bioinspired surface engineering: building blocks for liquid marbles and superhydrophobic surfaces, ACS Applied Materials & Interfaces 9 (2017) 7648–7657, https://doi.org/10.1021/acsami.6b16733.
- [13] C. Chakraborty, L. Leclercq, Y. Chen, Z. Liu, W. Yuan, Y. Yang, Z. Fang, X. Chen, W. Zhang, Y. Xie, An overview of pickering emulsions: Solid-particle materials, classification, morphology, and applications, Frontiers in Pharmacology 8 (2017) 287. https://doi.org/10.3389/fphar.2017.00287.
- [14] L.C. Bradley, K.J. Stebe, D. Lee, Clickable janus particles, Journal of the American Chemical Society 138 (2016) 11437–11440, https://doi.org/10.1021/ JACS.6B05633/ASSET/IMAGES/LARGE/JA-2016-05633Q_0005_JPEG.
- [15] W.H. Chen, F. Tu, L.C. Bradley, D. Lee, Shape-tunable synthesis of sub-micrometer lens-shaped particles via seeded emulsion polymerization, Chemistry of Materials. 29 (2017) 2685–2688, https://doi.org/10.1021/ACS.CHEMMATER.7B00494/ ASSET/IMAGES/LARGE/CM-2017-00494C 0006.JPEG.
- [16] B.Y. Guan, L. Yu, X. Wen, D. Lou, Formation of asymmetric bowl-like mesoporous particles via emulsion-induced interface anisotropic assembly, Journal of the American Chemical Society 138 (2016) 11306–11311, https://doi.org/10.1021/ iacs.6b06558.
- [17] J. Liu, A. Radja, Y. Gao, R. Yin, A. Sweeney, S. Yang, Mimicry of a biophysical pathway leads to diverse pollen-like surface patterns, Proceedings of the National Academy of Sciences of the United States of America 117 (2020) 9699–9705, https://doi.org/10.1073/PNAS.1919060117/-/DCSUPPLEMENTAL.
- [18] J.-W. Kim, R.J. Larsen, D.A. Weitz, Synthesis of nonspherical colloidal particles with anisotropic properties, Journal of the American Chemical Society 128 (2006) 14374–14377, https://doi.org/10.1021/ja065032m.
- [19] T. Fujibayashi, M. Okubo, Preparation and thermodynamic stability of micronsized, monodisperse composite polymer particles of disc-like shapes by seeded dispersion polymerization, Langmuir 23 (2007) 7958–7962, https://doi.org/ 10.1021/la7007842.
- [20] J.A. Champion, Y.K. Katare, S. Mitragotri, Making polymeric micro-and nanoparticles of complex shapes, Proceedings of the National Academy of Sciences. 104 (2007) 11901–11904, https://doi.org/10.1073/pnas.0705326104.
- [21] F. Chang, S. Ouhajji, A. Townsend, K. Sanogo Lacina, B.G.P. van Ravensteijn, W. K. Kegel, Controllable synthesis of patchy particles with tunable geometry and orthogonal chemistry, Journal of Colloid and Interface Science 582 (2021) 333–341, https://doi.org/10.1016/J.JCIS.2020.08.038.
- [22] S. Ravaine, E. Duguet, Synthesis and assembly of patchy particles: Recent progress and future prospects, Curr Opin Colloid Interface Science 30 (2017) 45–53, https://doi.org/10.1016/J.COCIS.2017.05.002.
- [23] D. Han, D.-L. Zhou, Q.-Y. Guo, X. Lin, Q. Zhang, Q. Fu, Engineering the surface pattern of microparticles: From raspberry-like to golf ball-like, ACS Applied Materials & Interfaces 13 (2021) 31215–31225, https://doi.org/10.1021/ acsami.1c08663.
- [24] X. Huang, L. Song, X. Jiang, X. Zhang, Fabrication and self-assembly of the tetrahedron dimpled colloidal particles Polymers & biopolymers, Journal of Materials Science 57 (2022) 7400–7415, https://doi.org/10.1007/s10853-022-07087-x
- [25] M. Zanini, C.P. Hsu, T. Magrini, E. Marini, L. Isa, Fabrication of rough colloids by heteroaggregation, Colloids and Surfaces. A, Physicochemical and Engineering Aspects 532 (2017) 116–124, https://doi.org/10.1016/J.COLSURFA.2017.05.084.
- [26] R.-K. Wang, H.-R. Liu, F.-W. Wang, Facile preparation of raspberry-like superhydrophobic polystyrene particles via seeded dispersion polymerization, Langmuir 29 (2013) 11440–11448, https://doi.org/10.1021/la401701z.
- [27] S. Trevenen, P.J. Beltramo, Gradient stretching to produce variable aspect ratio colloidal ellipsoids, Journal of Colloid and Interface Science 583 (2021) 385–393, https://doi.org/10.1016/j.jcis.2020.09.065.
- [28] U. Akiva, S. Margel, Surface-modified hemispherical polystyrene/polybutyl methacrylate composite particles, Journal of Colloid and Interface Science 288 (2005) 61–70, https://doi.org/10.1016/J.JCIS.2005.02.077.
- [29] T. Suzuki, H. Minami, W. Li, D. Suzuki, D. Minami, A facile method for preparation of polymer particles having a" cylindrical" shape, Angewandte Chemie International Edition. 57 (2018) 9936–9940, https://doi.org/10.1002/ ange.201805700.
- [30] T. Tanaka, M. Okayama, H. Minami, M. Okubo, Dual stimuli-responsive "mushroom-like" janus polymer particles as particulate surfactants †, Langmuir 26 (2010) 11732–11736, https://doi.org/10.1021/la101237c.
- [31] Y. Wang, W. Huang, L. Huang, S. Zhang, D. Hua, X. Zhu, Synthesis of walnut-like polystyrene particles using a "giant" surfactant and its superhydrophobic property, Polymer Chemistry 4 (2013) 2255–2259, https://doi.org/10.1039/c3py21142h.
- [32] S.C. Glotzer, M.J. Solomon, Anisotropy of building blocks and their assembly into complex structures, Nature Mater. 6 (2007) 557–562, https://doi.org/10.1038/
- [33] A.B. Pawar, I. Kretzschmar, Fabrication, assembly, and application of patchy particles, Macromolecular Rapid Communications 31 (2010) 150–168, https://doi. org/10.1002/MARC.200900614.
- [34] D.J. Kraft, R. Ni, F. Smallenburg, M. Hermes, K. Yoon, D.A. Weitz, A. van Blaaderen, J. Groenewold, M. Dijkstra, W.K. Kegel, Surface roughness directed selfassembly of patchy particles into colloidal micelles, Proceedings of the National Academy of Sciences. 109 (2012) 10787–10792, https://doi.org/10.1073/ pnas.1116820109.
- [35] S. Mitragotri, J. Lahann, Physical approaches to biomaterial design, Nature Materials 8 (2009) 15–23, https://doi.org/10.1038/nmat2344.

- [36] Q. Chen, J.K. Whitmer, S. Jiang, S.C. Bae, E. Luijten, S. Granick, Supracolloidal reaction kinetics of janus spheres, Science 331 (2011) 199–202, https://doi.org/ 10.1126/SCIENCE.1197451/SUPPL.FILE/CHEN.SOM.PDF.
- [37] F. Romano, E. Sanz, F. Sciortino, Phase diagram of a tetrahedral patchy particle model for different interaction ranges, The Journal of Chemical Physics 132 (2010) 184501, https://doi.org/10.1063/1.3393777.
- [38] F. Sciortino, Gel-forming patchy colloids and network glass formers: thermodynamic and dynamic analogies, European Physical Journal B: Condensed Matter and Complex Systems 64 (2008) 505–509, https://doi.org/10.1140/epjb/ e2008-00034-0.
- [39] R. Liang, X. Fang, B. Qiu, H. Zou, One-step synthesis of golf ball-like thiol-functionalized silica particles, Soft Matter 16 (2020) 9113–9120, https://doi.org/10.1039/d0sm01214a.
- [40] M. Zeng, D. King, D. Huang, C. Do, L. Wang, M. Chen, S. Lei, P. Lin, Y. Chen, Z. Cheng, Iridescence in nematics: Photonic liquid crystals of nanoplates in absence of long-range periodicity, Proceedings of the National Academy of Sciences. 116 (2019) 18322–18327, https://doi.org/10.1073/pnas.1906511116.
- [41] X. Chen, L. Song, X. Jiang, X. Zhang, Bioinspired superhydrophobic-superhydrophilic convertible film based on anisotropic red blood cell-like particles with protuberances, Colloids and Surfaces. A, Physicochemical and Engineering Aspects 579 (2019) 123674, https://doi.org/ 10.1016/J.COLSURFA.2019.123674.
- [42] M. Hu, C.P. Hsu, L. Isa, Particle surface roughness as a design tool for colloidal systems, Langmuir 36 (2020) 11171–11182, https://doi.org/10.1021/ACS. LANGMUIR.0C02050/ASSET/IMAGES/LARGE/LA0C02050_0003.JPEG.
- [43] L.C. Hsiao, S. Pradeep, Experimental synthesis and characterization of rough particles for colloidal and granular rheology, Curr Opin Colloid Interface Science 43 (2019) 94–112, https://doi.org/10.1016/J.COCIS.2019.04.003.
- [44] P.J. van Zwol, G. Palasantzas, J.M.T. De Hosson, Roughness corrections to the Casimir force: The importance of local surface slope, Applied Physics Letters 91 (2007) 144108, https://doi.org/10.1063/1.2795795.
- [45] D. Maria, L. Mammen, M. Singh, X. Deng, M. Roth, G.K. Auernhammer, H.J. Butt, D. Vollmer, Superhydrophobic surfaces by hybrid raspberry-like particles, Faraday Discussions 146 (2010) 35-48, https://doi.org/10.1039/c005270c.
- [46] U. Choudhury, L.S. Soler, J.G. Gibbs, S. Sanchez, P. Fischer, Surface roughnessinduced speed increase for active Janus micromotors, Chemical Communications 51 (2015) 8660–8663, https://doi.org/10.1039/c5cc01607j.
- [47] W. Chen, S. Tan, Z. Huang, T.-K. Ng, W.T. Ford, P. Tong, Measured long-ranged attractive interaction between charged polystyrene latex spheres at a water-air interface, Physical Review E 74 (2006) 021406, https://doi.org/10.1103/ PhysRevE.74.021406.
- [48] S. Trevenen, M.A. Rahman, H.S.C. Hamilton, A.E. Ribbe, L.C. Bradley, P. J. Beltramo, Nanoscale porosity in microellipsoids cloaks interparticle capillary attraction at fluid interfaces, ACS Nano 17 (2023) 11892–11904, https://doi.org/10.1021/ACSNANO.3C03301.
- [49] R. Van Hooghten, L. Imperiali, V. Boeckx, R. Sharma, J. Vermant, Rough nanoparticles at the oil-water interfaces: Their structure, rheology and applications, Soft Matter 9 (2013) 10791–10798, https://doi.org/10.1039/ C3SM52089G.
- [50] N. Sharifi-Mood, I.B. Liu, K.J. Stebe, Curvature capillary migration of microspheres, Soft Matter 11 (2015) 6768–6779, https://doi.org/10.1039/ c5sm00310e
- [51] G. Boniello, C. Blanc, D. Fedorenko, M. Medfai, N. Ben Mbarek, M. In, M. Gross, A. Stocco, M. Nobili, Brownian diffusion of a partially wetted colloid, Nature Materials 14 (2015) 908–911, https://doi.org/10.1038/nmat4348.
- [52] D. Ershov, J. Sprakel, J. Appel, M.A.C. Stuart J., van der gucht, capillarity-induced ordering of spherical colloids on an interface with anisotropic curvature, Proceedings of the National Academy of Sciences. 110 (2013) 9220–9224, https://doi.org/10.1073/pnas.1222196110.
- [53] J.B. Fournier, P. Galatola, Anisotropic capillary interactions and jamming of colloidal particles trapped at a liquid-fluid interface, Physical Review E 65 (2002) 31601, https://doi.org/10.1103/PhysRevE.65.031601.
- [54] H.M.H. Weijgertze, W.K. Kegel, M. Zanini, Patchy rough colloids as pickering stabilizers, Soft Matter 16 (2020) 8002–8012, https://doi.org/10.1039/ DOSMO0807A
- [55] A. San-Miguel, S.H. Behrens, Influence of nanoscale particle roughness on the stability of pickering emulsions, Langmuir 28 (2012) 12038–12043, https://doi. org/10.1021/LA302224V/SUPPL_FILE/LA302224V_SI_001.PDF.
- [56] C.J. Mable, N.J. Warren, K.L. Thompson, O.O. Mykhaylyk, S.P. Armes, Framboidal ABC triblock copolymer vesicles: A new class of efficient Pickering emulsifier, Chemical Science 6 (2015) 6179–6188, https://doi.org/10.1039/c5sc02346g.
- [57] M. Zanini, C. Marschelke, S.E. Anachkov, E. Marini, A. Synytska, L. Isa, Universal emulsion stabilization from the arrested adsorption of rough particles at liquidliquid interfaces, Nature Communications 8 (2017) 1–9, https://doi.org/10.1038/
- [58] Q. Xie, J. Harting, Controllable capillary assembly of magnetic ellipsoidal janus particles into tunable rings, Chains and Hexagonal Lattices, Advanced Materials. 33 (2021) 2006390, https://doi.org/10.1002/ADMA.202006390.
- [59] A. Donev, I. Cisse, D. Sachs, E.A. Variano, F.H. Stillinger, R. Connelly, S. Torquato, P.M. Chaikin, Improving the density of jammed disordered packings using ellipsoids, Science 303 (2004) 990–993, https://doi.org/10.1126/ SCIENCE.1093010/ASSET/09C1F4D9-86A5-4B6A-ABF6-C1C903CB600C/ ASSETS/GRAPHIC/ZSE0060422750004_JPEG.
- [60] B. Madivala, J. Fransaer, J. Vermant, Self-assembly and rheology of ellipsoidal particles at interfaces, Langmuir 25 (2009) 2718–2728, https://doi.org/10.1021/ la803554u.

- [61] M.R. Schure, R.S. Maier, Ellipsoidal particles for liquid chromatography: Fluid mechanics, efficiency and wall effects, Journal of Chromatography. A 1580 (2018) 30–48, https://doi.org/10.1016/J.CHROMA.2018.09.051.
- [62] Y. Wang, C. Li, X. He, J. Zhu, Preparation and assembly of concave polymer microparticles, RSC Advances 5 (2015) 36680–36686, https://doi.org/10.1039/ c5ra04110d.
- [63] X. Mao, M. Wang, S. Jin, J. Rao, R. Deng, J. Zhu, Monodispersed polymer particles with tunable surface structures: Droplet microfluidic-assisted fabrication and biomedical applications, Journal of Polymer Science. 60 (2022) 1653–1669, https://doi.org/10.1002/pol.20210909.
- [64] Y. Kawai, T. Yamamoto, Synthesis of dimpled and submicron-sized polymer particles of different morphologies using free micromixer, Colloids and Interface Science Communications. 32 (2019) 100193, https://doi.org/10.1016/J. COLCOM.2019.100193.
- [65] Y. Wang, L. Shang, Y. Zhao, L. Sun, Microfluidic generation of multicomponent soft biomaterials, Engineering 13 (2022) 128–143, https://doi.org/10.1016/J. ENG.2021.02.026.
- [66] Y.K. Takahara, S. Ikeda, K. Tachi, T. Sakata, T. Hasegawa, H. Mori, M. Matsumura, B. Ohtani, Porous polystyrene microspheres having dimpled surface structures prepared within micellar assemblies of amphiphilic silica particles in water, Chemical Communications. 33 (2005) 4205–4207, https://doi.org/10.1039/b507123b
- [67] K. Kadowaki, H. Ishii, D. Nagao, M. Konno, Imprinting dimples on narrowly dispersed polymeric spheres by heterocoagulation between hard polymer particles and soft oil droplets, Langmuir 32 (2016) 11600–11605, https://doi.org/10.1021/ acs.langmuir.6b02688.
- [68] V.N. Manoharan, M.T. Elsesser, D.J. Pine, Dense packing and symmetry in small clusters of microspheres, Science 301 (2003) 483–487, https://doi.org/10.1126/ SCIENCE.1086189/SUPPL FILE/MANOHARAN.SOM.PDF.
- [69] A.M. Yake, C.E. Snyder, D. Velegol, Site-specific functionalization on individual colloids: size control, stability, and multilayers, Langmuir 23 (2007) 9069–9075, https://doi.org/10.1021/la7011292.
- [70] A. Perro, S. Reculusa, S. Ravaine, E. Bourgeat-Lami, E. Duguet, Design and synthesis of Janus micro-and nanoparticles, Journal of Materials Chemistry 15 (2005) 3745–3760, https://doi.org/10.1039/b505099e.
- [71] J. Li, R.K. Ulrich, B.H. Mcclintock, A.A. Norton, J. Li, E.O. Ogundimu, E. T. Akinlabi, C.A. Mgbemene, D.-X. Ye, Y.-P. Zhao, G.-R. Yang, Y.-G. Zhao, G.-C. Wang, T.-M. Lu, Manipulating the column tilt angles of nanocolumnar films by glancing-angle deposition, Nanotechnology 13 (2002) 615–618.
- [72] M. Yu, Q. Wang, M. Zhang, Q. Deng, D. Chen, Facile fabrication of raspberry-like composite microspheres for the construction of superhydrophobic films and applications in highly efficient oil-water separation, RSC Advances 7 (2017) 39471–39479, https://doi.org/10.1039/c/ra07250c.
- [73] Z. Qian, Z. Zhang, L. Song, H. Liu, A novel approach to raspberry-like particles for superhydrophobic materials, Journal of Material Chemistry 19 (2009) 1297–1304, https://doi.org/10.1039/b810808k.
- [74] M. Okubo, Y. Murakami, T. Fujiwara, Formation mechanism of anomalous "golf ball-like" composite polymer particles by seeded emulsion polymerization, Colloid & Polymer Science 274 (1996) 520–524, https://doi.org/10.1007/BF00655226/METDICS
- [75] N. Konishi, T. Fujibayashi, T. Tanaka, H. Minami, M. Okubo, Effects of properties of the surface layer of seed particles on the formation of golf ball-like polymer particles by seeded dispersion polymerization, Polymer Journal 42 (2010) 66–71, https://doi.org/10.1038/pi.2009.313.
- [76] G. Russo, M. Lattuada, Synthesis of non-spherical polymer particles using the activated swelling method, Journal of Colloid and Interface Science 611 (2022) 377–389, https://doi.org/10.1016/J.JCIS.2021.11.082.

- [77] H. Gui, Y. Li, D. Du, Q. Bo Meng, X.M. Song, F. Liang, Preparation of asymmetric particles by controlling the phase separation of seeded emulsion polymerization with ethanol/water mixture, Journal of Colloid and Interface Science 618 (2022) 496–506, https://doi.org/10.1016/J.JCIS.2022.03.081.
- [78] D.J. Kraft, J. Hilhorst, M.A.P. Heinen, M.J. Hoogenraad, B. Luigjes, W.K. Kegel, Patchy polymer colloids with tunable anisotropy dimensions, Journal of Physical Chemistry B. 115 (2011) 7175–7181, https://doi.org/10.1021/JP108760G/ SUPPL_FILE/JP108760G_SL_001.PDF.
- [79] Z.-W. Li, Y.-L. Zhu, Z.-Y. Lu, Z.-Y. Sun, General patchy ellipsoidal particle model for the aggregation behaviors of shape-and/or surface-anisotropic building blocks, Soft Matter 14 (2018) 7625–7633, https://doi.org/10.1039/c8sm01631c.
- [80] A.A. Shah, B. Schultz, K.L. Kohlstedt, S.C. Glotzer, M.J. Solomon, Synthesis, assembly, and image analysis of spheroidal patchy particles, Langmuir 29 (2013) 4688–4696, https://doi.org/10.1021/la400317t.
- [81] J.G. Lee, A. Al Harraq, K.J.M. Bishop, B. Bharti, Fabrication and electric field-driven active propulsion of patchy microellipsoids, The Journal of Physical Chemistry. B 125 (2021) 4232–4240, https://doi.org/10.1021/acs.jpcb.1c01644.
- [82] Z. Zhang, P. Pfleiderer, A.B. Schofield, C. Clasen, J. Vermant, Synthesis and directed self-assembly of patterned anisometric polymeric particles, Journal of the American Chemical Society 133 (2011) 392–395, https://doi.org/10.1021/ iol.09000.
- [83] L. Tian, X. Li, D. Wan, Z. Ali, Q. Zhang, Large-scale fabrication of polymer ellipsoids with controllable patches via the viscosity-induced deformation of spherical particles, Polymer Chemistry 8 (2017) 3774–3777, https://doi.org/ 10.1039/c7py00475c.
- [84] V.N. Paunov, Novel method for determining the three-phase contact angle of colloid particles adsorbed at air—water and oil—water interfaces, Langmuir 19 (2003) 7970–7976, https://doi.org/10.1021/LA0347509.
- [85] A.D. Nikolov, D.T. Wasan, A. Chengara, K. Koczo, G.A. Policello, I. Kolossvary, Superspreading driven by marangoni flow, Advances in Colloid and Interface Science 96 (2002) 325–338, https://doi.org/10.1016/S0001-8686(01)00087-2.
- [86] D. Nečas, P. Klapetek, Gwyddion: An open-source software for SPM data analysis, Central European Journal of Physics. 10 (2012) 181–188, https://doi.org/ 10.2478/S11534-011-0096-2/MACHINEREADABLECITATION/RIS.
- [87] H.S.C. Hamilton, L.C. Bradley, Probing the morphology evolution of chemically anisotropic colloids prepared by homopolymerization- and copolymerizationinduced phase separation, Polymer Chemistry 11 (2020) 230–235, https://doi.org/ 10.1039/c9nv01166h.
- [88] Z. Luo, Yitong Li, B. Liu, Colloidal particles with complex microstructures via phase separation in swelled polymer microspheres, Chemical Communications. 53 (2017) 8649–8652. https://doi.org/10.1039/c7cc04147k.
- [89] J. Liao, C. Zhu, Z. He, J. Zhang, Y. Zeng, Z. Gu, Kinetically controlled synthesis of nonspherical polystyrene nanoparticles with manipulatable morphologies, Langmuir 38 (2022) 12132–12139, https://doi.org/10.1021/ACS. LANGMUIR.2C01326/SUPPL FILE/LA2C01326 SI 001.PDF.
- [90] M. Okubo, T. Miya, H. Minami, R. Takekoh, Morphology of micron-sized, monodisperse, nonspherical polystyrene/poly(n-butyl methacrylate) composite particles produced by seeded dispersion polymerization, Journal of Applied Polymer Science 83 (2002) 2013–2021, https://doi.org/10.1002/APP.10158.
- [91] F. Chang, B.G.P. Van Ravensteijn, K.S. Lacina, W.K. Kegel, Bifunctional janus spheres with chemically orthogonal patches, ACS Macro Letters 8 (2019) 714–718, https://doi.org/10.1021/acsmacrolett.9b00193.
- [92] M. Fernández-García, J.L. De la Fuente, M.L. Cerrada, E.L. Madruga, Preparation of poly(tert-butyl acrylate-g-styrene) as precursors of amphiphilic graft copolymers. 1. Kinetic study and thermal properties, Polymer (Guildf) 43 (2002) 3173–3179, https://doi.org/10.1016/S0032-3861(02)00140-4.